Natland, J.H., Dick H.J.B., Miller, D.J., and Von Herzen, R.P. (Eds.)
Proceedings of the Ocean Drilling Program, Scientific Results Volume 176

12. Major and Trace Element Evolution of Hole 735B Gabbros[1]

Jonathan E. Snow[2]

ABSTRACT

Sixty-three major and trace element analyses from Hole 735B reflect known characteristics of the igneous and metamorphic evolution of the oceanic crust at this site. Regular association of ferrogabbro formation with more evolved units suggests either intrusion into a crystal mush (residual melt porosity) or the tectonic incompetence of the evolved units (fracture generated porosity). Relationships of the titanophile elements (Zr, Y, and V) can "fingerprint" magma-crystallizing mineral phases in which these elements are compatible. In this way, a high V, low Zr and Y oxide-crystallizing magma can be clearly distinguished from the main magmatic trend, and a general concentration of high-Zr magmas is found near the top of the hole. This suggests independently of the stratigraphy that different magmas were responsible for the various magmatic cycles. Results of the analyses additionally form the basis for further study of the bulk chemistry of the magmas that formed this locality.

INTRODUCTION

Ocean Drilling Program (ODP) Hole 735B is the first and only long, continuous section of lower oceanic crust ever sampled. It is located on the Southwest Indian Ridge at 57°E and begins near the top of the gabbroic section, extending nearly to its bottom (Dick et al., 1991; Dick et al., 2000; Dick et al., 1999). This 1500-m-long section has proven quite useful for studies involving the igneous evolution of the oceanic crust, its metamorphic evolution, and its post-subduction role as a reservoir of trace elements within the mantle (Snow et al., 1999, unpubl. data).

[1]Snow, J.E., 2002. Major and trace element evolution of Hole 735B gabbros. *In* Natland, J.H., Dick, H.J.B., Miller, D.J., and Von Herzen, R.P. (Eds.), *Proc. ODP, Sci. Results,* 176, 1–18 [Online]. Available from World Wide Web: <http://www-odp.tamu.edu/publications/176_SR/VOLUME/CHAPTERS/SR176_12.PDF>. [Cited YYYY-MM-DD]
[2]Max-Planck Institut für Chemie, Postfach 3060, 55020 Mainz, Federal Republic of Germany. **jesnow@mpch-mainz.mpg.de**

Initial receipt: 15 May 2000
Acceptance: 8 August 2002
Web publication: 24 October 2002
Ms 176SR-010

This paper reports on the major and trace element compositions of 60 gabbroic samples from the drill core. These analyses lay the groundwork for further study of the core by bulk geochemical means.

Hole 735B consists of one or more cumulate stacks of nearly cotectic olivine-plagioclase-clinopyroxene cumulates with minor orthopyroxene in some sections that lack olivine (Dick et al., 1991). This cumulate stack is reintruded by highly evolved liquids that crystallized further plagioclase and pyroxene, along with large amounts of iron and titanium oxides. The cumulate sequences are themselves cut by primitive olivine microgabbros and by late-stage silicic melts (Dick et al., 2000, 1999).

SAMPLING

There are three sets of samples in this study. One is a set of gabbros sampled on board the *JOIDES Resolution* during the course of Leg 176. Another is a set from Leg 118 (R. Emmermann, pers. comm., 1998), and finally, a set of three muds from the core splitting table. With the exception of the muds, all of the samples were chosen to be representative of major rock types and units and an effort was made to include all the major gabbroic lithologies. No attempt was made to sample felsic veins, as other investigators have adequately sampled these.

However careful a point-sampling program is, it is impossible to generate a perfectly representative sampling of a section. This is particularly true in the case of cumulate rocks, where small lithologic units with very high concentrations of some elements will dominate the average and may or may not be included proportionately in the mean. For this reason, it was decided to subsample the mud from the onboard saw table as a means of estimating the bulk composition of the hole. Details of the philosophy and practice behind this sampling are published elsewhere (Snow et al., 1999, unpubl. data).

METHODS

The samples were cut from quater-core sections that were cleaned in an ultrasonic bath and oven-dried at 80°C. The samples were precrushed by being wrapped in thick plastic sheeting and struck repeatedly with a 2.5-kg mechanic's hammer. Chips of fresh material with only broken surfaces of a total of 50–100 g were selected for further crushing, and the rest were put aside for future mineral separation. In this way surface contamination from drilling fluids and saw marks can be avoided in the whole-rock powder. The chips were then further crushed using an agate shatterbox and recrushed as necessary to obtain a fine powder without detectable graininess.

Major and trace elements were measured in the samples at the Universität Mainz using a Philips PW 1404 X-ray fluorescence spectrometer (Groschopf, 1997). Major elements were measured on $LiBO_4$-fused glass disks, and trace elements were measured on pressed powder pellets. USGS reference standard BCR-1 was measured as an external control on the trace elements. The data are listed in Table T1.

T1. Major and trace element analyses, p. 15.

RESULTS

Major Elements

The major elements presented here agree closely with the shipboard measurements and fairly clearly reflect the igneous evolution of the region surrounding the hole. The Mg numbers ($Mg^{2+}/[Mg^{2+}+Fe^{2+}]$) of the gabbros reflect the basic magmatic evolution of the cumulate pile (Fig. F1). They show the interfingering of differently evolved lavas and the reintrusion of the crystal mush by highly evolved iron-rich magmas. Figure F1 shows the evolution of the Mg number with depth in the hole. The data from the current study agree well with the shipboard measurements and reflect as well the major magmatic segmentation seen in the shipboard results. Also visible in Figure F1 are the ferrogabbros, with significantly lower Mg numbers. In Figure F1, only ferrogabbros from this study are shown. Samples with >0.5 wt% TiO_2 have been filtered out of the other two data sets for clarity. The ferrogabbros occur in two varieties: as gabbros bearing disseminated oxide grains and as massive oxides infiltrating the grain matrix of the gabbro.

Ferrogabbro intrusion into the crystal mush sequence is documented by variations in Fe_2O_3 and TiO_2, as shown in Figure F2. The correlation of Fe_2O_3 with TiO_2 is a sign of the involvement of ilmenite and titanomagnetite as crystallizing phases. The lack of a perfect correlation is because of multiple intrusion at different Fe_2O_3/TiO_2 ratios in the intruding magma, intrusion into country rocks of differing Fe_2O_3 contents, and differing liquidus mineralogy of the intruding magmas.

Trace Elements

Trace elements in the Hole 735B cumulate sequence reflect the same two themes just mentioned: magmatic differentiation as a cotectic cumulate followed by reintrusion of highly evolved liquids that crystallize oxides. This sequence can be best illustrated by plotting TiO_2 against Ni, as in Figure F3. In all of the Hole 735B gabbros, significant deposition of TiO_2-rich minerals appears only to have occurred in rocks with less than ~180 ppm Ni (Fig. F3). This observation has two main implications for the evolution of the magmatic sequence.

The ferrogabbros show a variety of intrusive relationships with the country rock. These range from graded or sutured contacts with more evolved units to sharper contacts with more primitive, more olivine-rich rocks. This suggests that there was a “crystallization wall” at ~180 ppm Ni that represented the state of solidification of the magmatic body as the reintrusion. Thus, the primitive cumulates must have been solid at the time of intrusion of the oxides, whereas the more evolved cumulate assemblages (with a lower solidus temperature) were still partially molten and amenable to infiltration.

The melts must have been autogenous. Had the evolved melts been generated elsewhere and only penetrated the cumulate sequence by chance, then it is unlikely that only evolved units would have been intruded. The nonrandom association of oxide-rich reintrusion with more evolved rocks suggests that instead the oxide-bearing magmas are derived from the cumulate sequence they intrude.

Other oxides than Fe_2O_3 also correlate with TiO_2, some in fact much better. Here such elements are termed titanophile elements and may be able to deliver clues to the origin of the magmas that deposited oxides

F1. Mg number vs. depth, Site 735, p. 8.

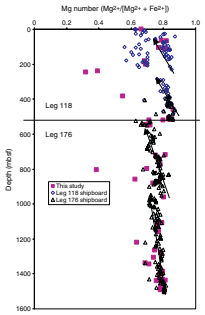

F2. TiO_2 vs. Fe_2O_3 in Hole 735B gabbros, p. 9.

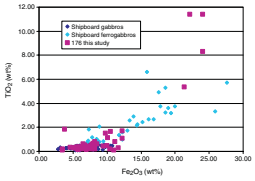

F3. Ni-TiO_2 relationships in Hole 735B gabbros, p. 10.

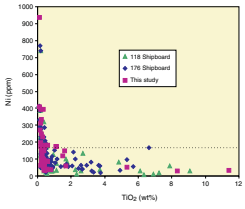

in the rock. A case in point is V, where the highest concentrations in ferrogabbros are a factor of 8–10 higher in the most Ti-rich rocks than they are in the background gabbros. Figure **F4** shows the relationship between TiO_2 and V in the Hole 735B gabbros. Although the two elements are clearly correlated through a very large concentration range, the V/Ti ratio is clearly variable. This suggests that the evolved magmas had variable Ti/V or that different minerals played a role in the oxide ores that were deposited. If so, this may have had a variety of causes.

Additional titanophile elements include Zr and Y. Interestingly, Sc correlates well with all of these elements in the less evolved gabbros and microgabbros. This is probably because of the compatibility of all of these elements in clinopyroxene. There is no correlation, however, between Sc and Mg, Mg number, or Ca number. Apparently, Sc is not compatible in oxides, as it is not correlated with Ti (Fig. **F5**).

In order to assess the contributions of different magmas to the formation of the oxide gabbros, it is instructive to consider the titanophile elements V, Y, and Zr as a "fingerprint" of the melt that crystallized the oxide phases. These elements are all compatible in oxides; thus, just as incompatible elements in basalts record the trace element ratios in their source, these three elements should largely retain their relative concentrations present in the liquid they crystallized from. A constant and regular variation in these elements is visible in the non-ferrogabbros, and it is assumed that this can be subtracted to yield only the excess contained in oxide.

Sc is a particularly useful element for assessing the baseline concentration for the titanophile elements. Like them, Sc is compatible in clinopyroxene, but is not enriched in the oxide phases. Figure **F5** shows Sc plotted against TiO_2. Sc was measured only in samples from this study, not in either shipboard data set. There is no particular enrichment of Sc in any of the high-Ti samples. Even in the oxide-richest sample at ~15% oxide, the Sc content is nearly within the range of nonoxide gabbros. For example, this means that the TiO_2 baseline can very clearly be established. The same is true of the other titanophile elements. When this is done, nearly constant silicate baselines can be established for TiO_2 (0.5 wt%), Zr and Y (both 15 ppm), and V (200 ppm).

Some trends in the data can be observed by looking at the ratios of the elements Zr, Y, and V together. The reasoning behind doing so is that different groupings of these elements in the oxide-bearing magmas would tend to "fingerprint" the magmas, possibly resulting in the identification of multiple magmatic events.

A sensible way to do this is to first subtract out the silicate "baseline" of 200 ppm V and 15 ppm each Zr and Y from each sample. Since the variations of these elements are small along the silicate evolution trend, this does not introduce significant scatter in the data. Then each data point is divided by the range (maximum – minimum) of that element in the data set: 1524 ppm for Zr, 130 ppm for Y, and 235 ppm for V. That way each analysis can have a value between 0 (the minimum in the data set) and 1 (the maximum in the data set). These values can thus be considered dimensionless. Figure **F6** shows a ternary diagram of the data normalized in this way. In this diagram, a major broad grouping is visible between the bulk of the samples in a broad band across the top of the diagram and a group of four high-V samples. As is clear from Figure **F4**, these are not the only samples with high V content but they are the only high-V samples where Zr and Y are also low. As there is little fractionation of these elements to be expected from the crystalliza-

F4. V vs. TiO_2, Hole 735B gabbros, p. 11.

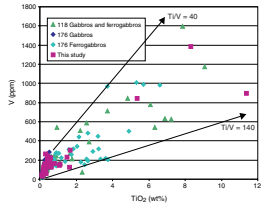

F5. Sc vs. TiO_2, p. 12.

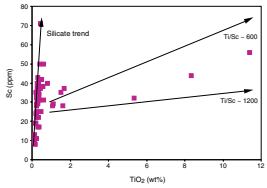

F6. Dimensionless titanophile elements in Hole 735B, p. 13.

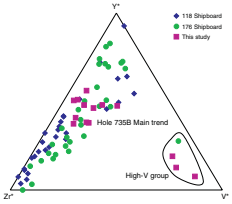

tion of oxide phases, it is possible that these four samples represent a completely separate oxide gabbro magma.

The remainder of the samples are plotted in Figure F7. These samples are grouped by depth in the section in order to see if any trends in relative titanophile content are depth dependent. The normalized analyses group in a broad band that stays close to constant relative V*/Y* (Fig. F7). The samples with the highest relative Zr contents tend to occur in the upper 300 m (lithologic Units X–Z), whereas in the lower part of the section Y and V tend to dominate over Zr. However, the overlap between the different depth intervals makes it difficult to draw firm additional conclusions about potential magmatic sources.

It is important to note that the phases precipitated from the reintruding liquids are themselves cumulates. A residual melt bearing much of the incompatible elements such as K and Rb has clearly been efficiently extracted from the ferrogabbros as well. Few of the ferrogabbros have more than a few tenths of a percent K_2O or P_2O_5. Even though they precipitated from highly evolved liquids, the oxide-rich gabbros must themselves have lost this component to still more highly evolved magma. This magma may be the one recorded in leucocratic and even granitic veins that cut the whole sequence.

F7. Dimensionless Zr-Y-V, without high-V, p. 14.

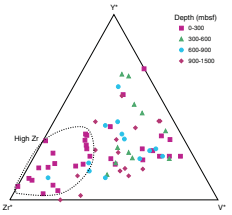

Microgabbros

A total of, 19 microgabbros were sampled for this study. Particular care was taken sampling the microgabbros, as their texture suggests that they may be liquid compositions and they are overall more mafic than the average for the core. Indeed, several of the microgabbros have elevated contents of P_2O_5 and K_2O, suggesting that they are not cumulates but instead represent liquid compositions. These may thus prove useful starting points for the evaluation of the overall liquid line of descent of the sequence.

CONCLUSIONS

New major and trace element results from ODP Hole 735B reflect the magmatic trends seen in the larger overall sampling conducted shipboard. Multiple magmatic mega-units a few hundred meters across show consistent magmatic trends and are crosscut by primitive microgabbros as well as highly evolved oxide-rich and silicic units. The "crystallization wall" at 180 ppm Ni suggests that primitive gabbros could not be wetted by the highly evolved liquids. Either they were too completely crystallized (retaining no residual melt porosity) or when in a crystalline state they were too mechanically competent to become conduits for melt migration (fracture porosity). The distinct fingerprint of several high-V samples is the first direct geochemical evidence of multiple magmas with multiple liquid lines of descent and reconfirms a major interpretation of the geochemical results to date.

ACKNOWLEDGMENTS

The author would like to thank Captain Ed Oonck and the crew of the *JOIDES Resolution*, as well as the co-chief scientists and shipboard scientific party for their professionalism and hard work during Leg 176. This research used samples and/or data provided by the Ocean Drilling

Program (ODP). ODP is sponsored by the U.S. National Science Foundation (NSF) and participating countries under management of Joint Oceanographic Institutions (JOI), Inc.

REFERENCES

Dick, H.J.B., Meyer, P.S., Bloomer, S., Kirby, S., Stakes, D., and Mawer, C., 1991. Lithostratigraphic evolution of an in-situ section of oceanic Layer 3. *In* Von Herzen, R.P., Robinson, P.T., et al., *Proc. ODP, Sci. Results,* 118: College Station, TX (Ocean Drilling Program), 439–538.

Dick, H.J.B., and Shipboard Party of Leg 176, 2000. A long in situ section of the lower ocean crust: results of ODP Leg 176 drilling at the Southwest Indian Ridge. *Earth Planet. Sci. Lett.,* 179:31–51.

Groschopf, N., 1997. Die Röntgenfluoreszenzanalyse. Quantitative Chemische Röntgenanalyses, Mineralogie, Uni-Mainz. <http://www.uni-mainz.de/FB/Geo/Geologie/EMSRFA/RFA.html>.

Shipboard Scientific Party, 1999. Leg 176 summary. *In* Dick, H.J.B., Natland, J.H., Miller, D.J., et al., *Proc. ODP, Init. Repts.,* 176: College Station, TX (Ocean Drilling Program), 1–70.

Snow, J.E., Jochum, K.P., and Hoefs, J., 1999. Does the "gabbroic" component in Hawaiian lavas come from ocean crust? *Eos, Trans.,* 80:1184. (Abstract)

Figure F1. Mg number vs. depth, Site 735. Arrows show inferred major magmatic trends. Shipboard data from Legs 176 and 118 do not include ferrogabbros.

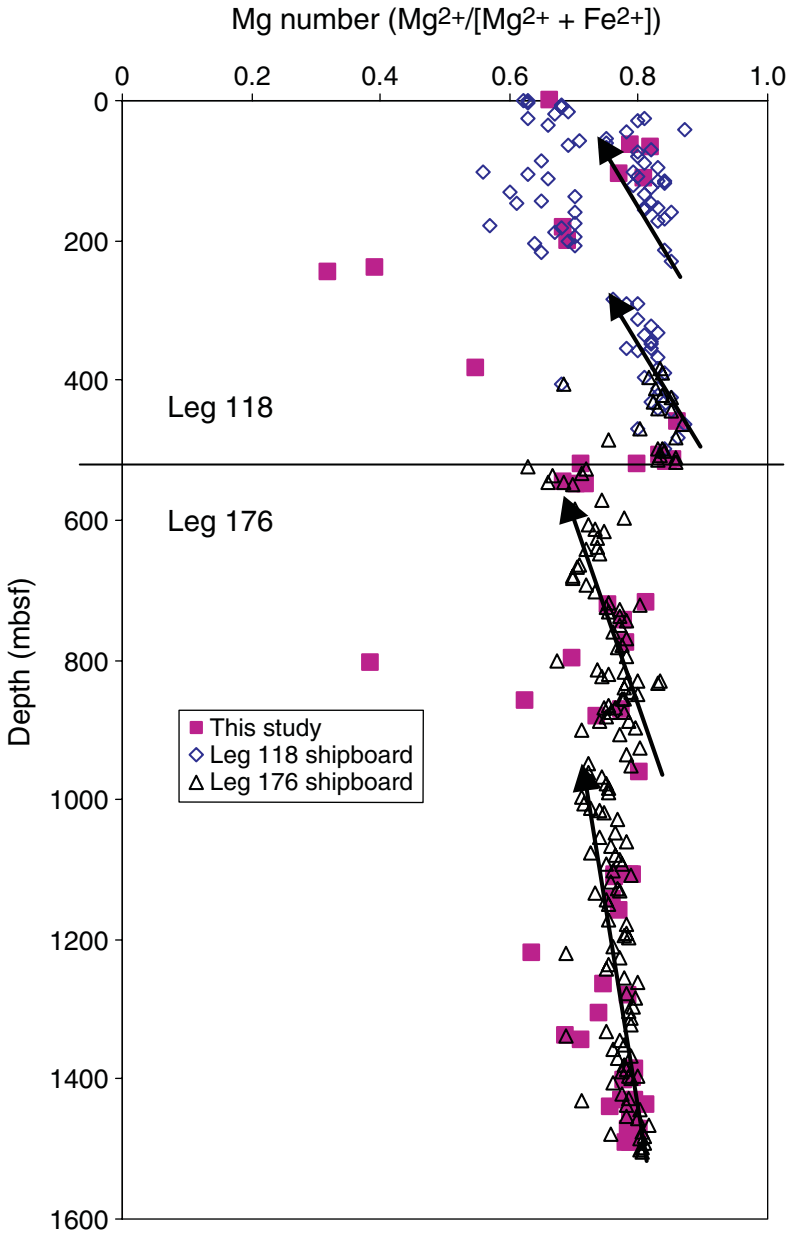

Figure F2. TiO_2 vs. Fe_2O_3 in Hole 735B gabbros. Differing slopes of the low-Fe and high-Fe portions of the diagram suggest that intruding magmas crystallized ilmenite with varying TiO_2/Fe_2O_3.

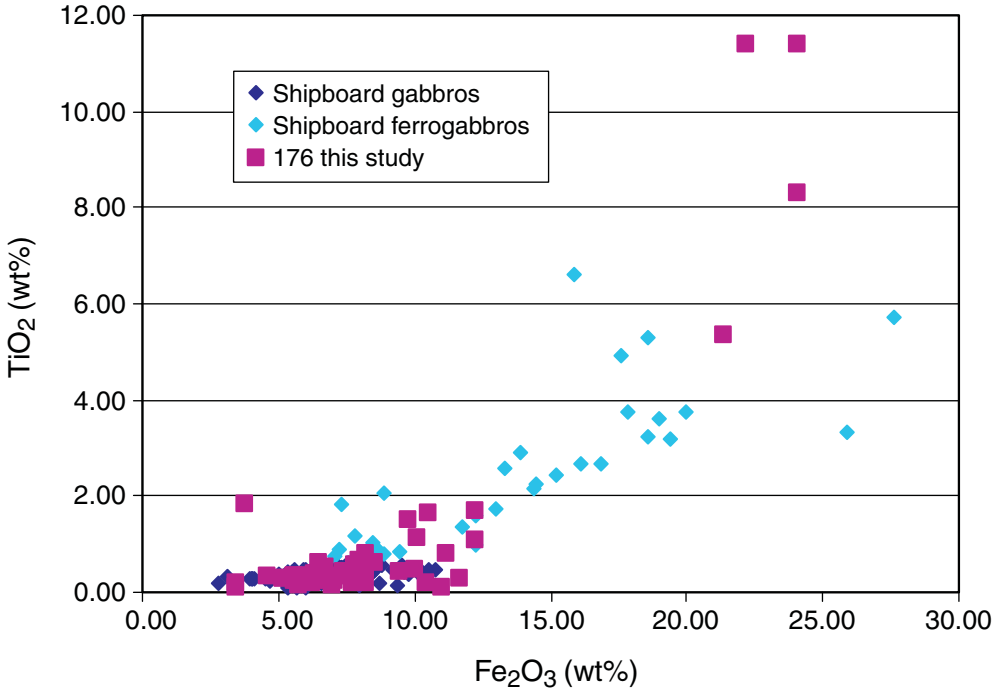

Figure F3. Ni-TiO_2 relationships in Hole 735B gabbros. High TiO_2 occurs only in more evolved compositions.

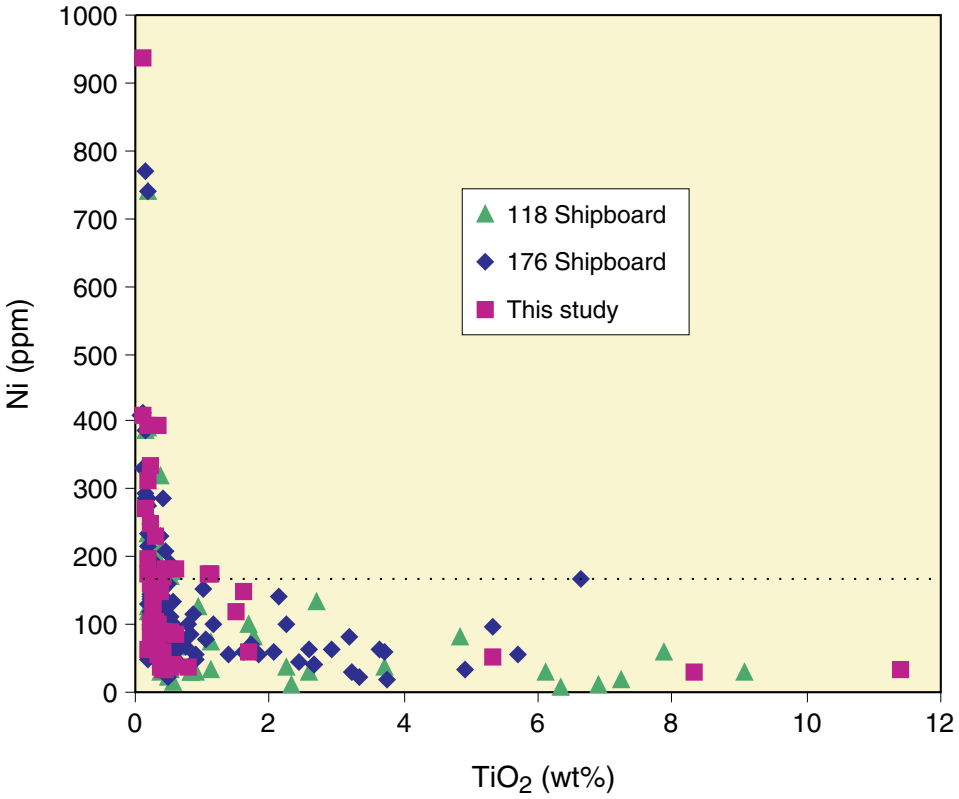

Figure F4. V vs. TiO_2, Hole 735B gabbros. Intrusion of variable Ti/V magmas into variably evolved preexisting cumulates is evident in the wide scatter of the data. Upper arrow shows a Ti/V of 40, the lower shows a Ti/V of 140.

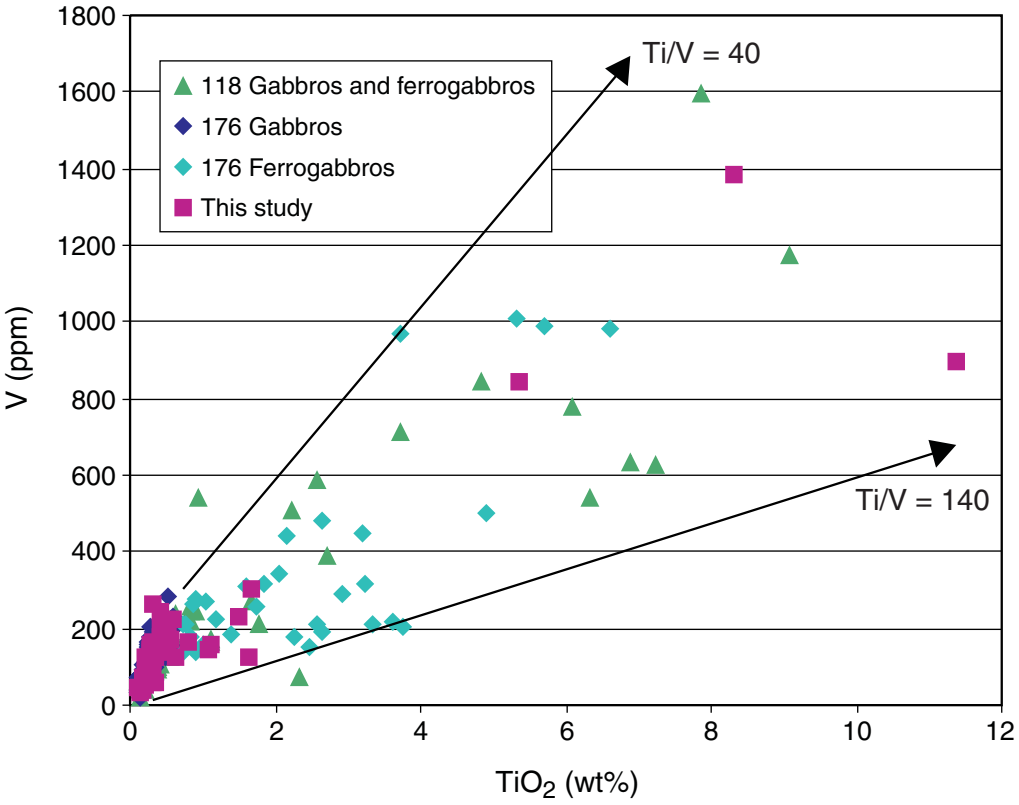

Figure F5. Sc vs. TiO_2. Note that Sc was not measured on board during Leg 118 or 176. A TiO_2 content of 0.5 wt% can readily be established as a baseline silicate contribution. Arrows show the expected effect of crystallization of oxides with Ti/Sc of 600 (lower arrow) to 1200 (upper arrow).

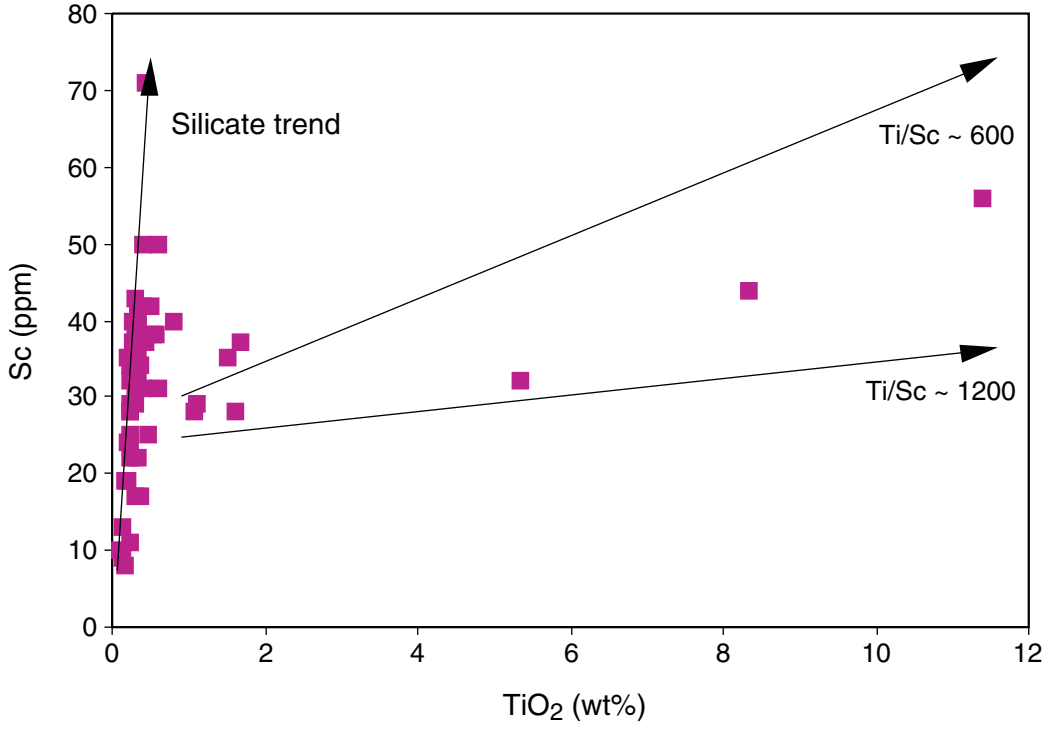

Figure F6. Dimensionless titanophile elements in Hole 735B ferragabbros, grouped by data set. Data are only from samples with >0.5 wt% TiO_2. "Silicate" contents of 200 ppm V and 15 ppm each Zr and Y have been subtracted out and the data renormalized to their ranges in the data sets.

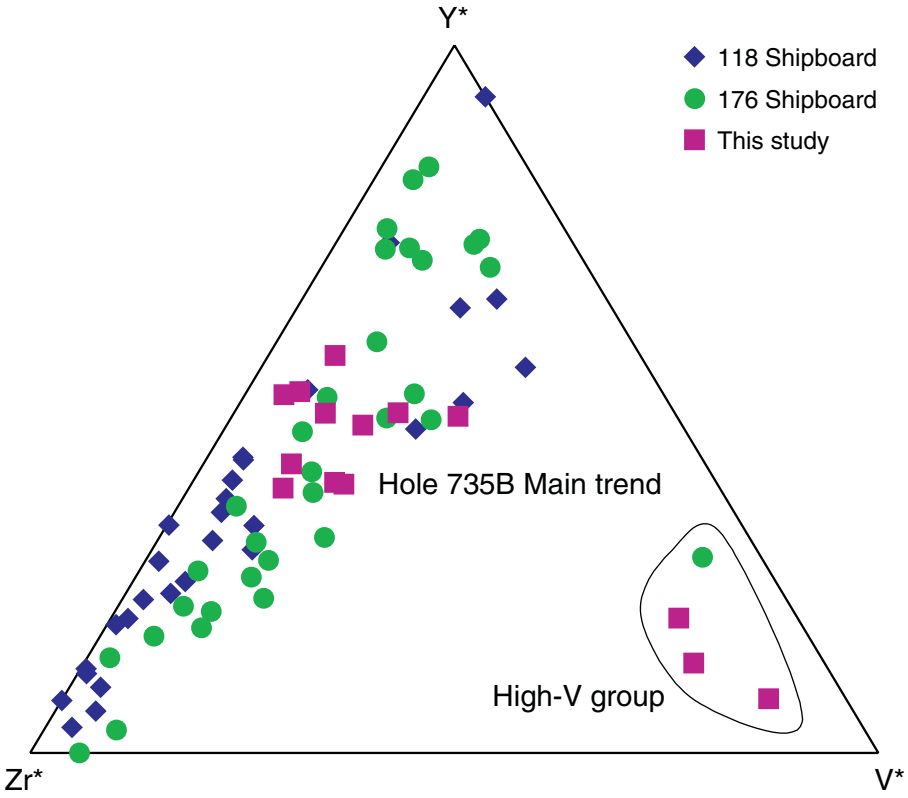

Figure F7. Dimensionless Zr-Y-V, without high-V samples grouped by depth. Calculated as in Figure F6, p. 13. Symbols correspond to depth in meters below seafloor as shown.

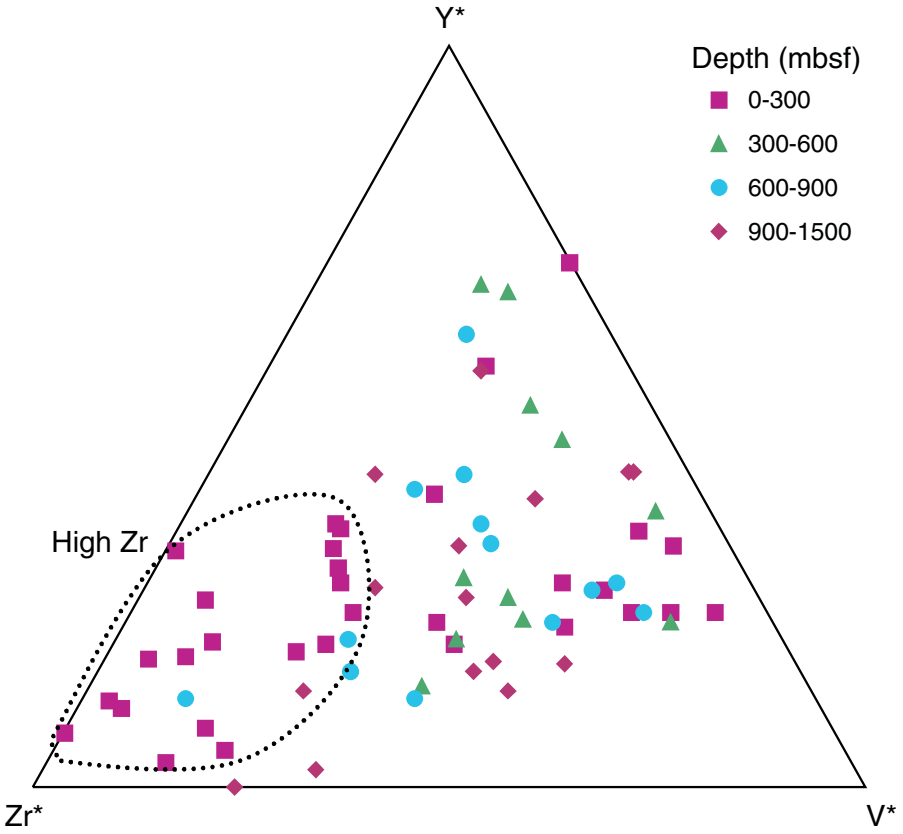

Table T1. Major element oxide and trace element analyses. (**See table notes.** Continued on next three pages.)

Core, section, interval (cm)	Depth (mbsf)	Thin section number	Rock type	Major element oxides (wt%)													
				SiO_2	Al_2O_3	Fe_2O_3	MnO	MgO	CaO	Na_2O	K_2O	TiO_2	P_2O_5	Cr_2O_3	NiO	LOI	Total
176-735B-																	
1R-1, 35–37	0.4	227	Olivine basalt	49.12	15.84	9.76	0.16	8.19	10.97	3.08	0.22	1.5	0.15	0.0471	0.0153	1.56	100.61
16R-2, 5–10	63.1	219	Olivine gabbro	50.57	17.63	5.98	0.11	9.49	12.82	2.9	0.03	0.31	0.01	0.0306	0.0146	1.2	101.09
16R-5, 38–40	66.8	220	Olivine microgabbro	47.71	16.12	6.22	0.1	12.04	12.58	2.46	0.12	0.24	0.03	0.1732	0.034	1.79	99.61
23R-5, 3–5	104.9	232	Diabase	50.67	17.4	7.09	0.12	10.13	11.59	3.14	0.03	0.33	0.01	0.0555	0.0215	1.09	101.68
25R-2, 104–107	113.3	234	Olivine gabbro	50.58	16.7	5.56	0.1	10.13	13.38	2.74	0.06	0.35	0.01	0.058	0.0215	0.94	100.62
38R-2, 24–26	182.5	257	Troctolitic micrograbbro	49.4	17.52	10.09	0.16	9.34	11.59	3.16	0.09	1.11	0.02	0.0542	0.269	0.05	102.6
41R-4, 22–27	199.7	260	Olivine gabbro	52.83	15.58	8.26	0.15	7.97	11.07	3.75	0.06	0.52	0.01	0.0027	0.0049	0.26	100.47
50R-1, 82–90	238.8	272	Oxide gabbro	38.87	9.87	22.2	0.28	6.15	8.4	2.78	0.05	11.39	0.01	0.005	0.0039	–0.51	99.48
51R-2, 16–25	244.5	274	Oxide gabbro	39.45	11.99	24.08	0.25	4.86	7.53	3.29	0.08	8.32	0.01	0.0064	0.005	–0.3	99.55
74R-6, 115–119	382.9	200	Olivine microgabbro	50.61	14.48	12.23	0.21	6.35	10.06	3.85	0.08	1.67	0.08	0.0253	0.0076	–0.13	99.51
83R-7, 115–120	461.1	213	Troctolite	42.82	9.38	11.05	0.16	29.08	5.84	1.01	0.05	0.1	0.01	0.0778	0.1245	0.89	100.58
90R-1, 126–137	509.1	126	Troctolitic gabbro	47.44	20.53	5.74	0.08	12.18	11.12	2.3	0.02	0.15	0.01	0.0308	0.0413	0.33	99.97
90R-6, 28–38	514.8	28	Troctolitic gabbro	46.92	17.08	6.25	0.1	15.51	10.78	2	0.11	0.2	0.01	0.096	0.0561	1.09	100.21
90R-8, 47–52	517.3	47	Olivine gabbro	45.93	17.86	7.02	0.1	16.39	9.01	2.07	0.05	0.13	0.01	0.0089	0.0545	0.54	99.19
91R-1, 43–53	517.8	43	Troctolitic gabbro	46.04	17.51	6.47	0.1	15.27	11.73	1.78	0.03	0.33	0.02	0.1441	0.0537	0.73	100.22
91R-2, 26–32	519.0	26	Troctolitic gabbro	52.52	16.22	7.41	0.14	7.83	11.92	3.79	0.08	0.43	0.01	0.003	0.0043	–0.01	100.33
91R-2, 101–110	519.8	101	Troctolitic gabbro	45.81	18.72	8.2	0.12	13.81	9.11	2.28	0.2	0.17	0.01	0.0067	0.0474	1.22	99.69
95R-2, 93–97	546.9	R2	Troctolitic gabbro	52.55	16.34	8.23	0.16	7.59	10.91	3.77	0.05	0.45	0	0.0026	0.0043	0	100.05
96R-1, 25–33	548.9	R1a	Microgabbro	52.44	16.41	7.63	0.14	7.81	11.43	3.77	0.06	0.42	0.01	0.0027	0.0051	0.31	100.45
96R-1, 82–84	549.1	R1b	Microgabbro	50.7	7.69	11.14	0.24	12.16	15.16	1.75	0.06	0.79	0.06	0.0803	0.0228	0.74	100.59
121R-1, 14–19	719.8	R1c	Olivine gabbro	51.53	16.88	5.17	0.1	9.62	13.83	2.66	0.02	0.29	0	0.0289	0.013	0.21	100.36
121R-3, 65–75	723.3	65a	Microgabbro	51.39	15.89	6.78	0.01	8.94	12.18	3.34	0.05	0.53	0.04	0.0261	0.0132	0.93	100.23
123R-4, 83–89	744.0	R4a	Troctolitic gabbro	49.72	18.05	6.87	0.11	10.41	11.49	2.89	0.03	0.25	0.02	0.0343	0.0175	0.22	100.11
128R-3, 6–12	777.5	6	Microgabbro	50.23	16.4	6.48	0.12	9.85	13.07	2.63	0.03	0.29	0	0.0447	0.0142	0.75	99.91
130R-5, 10–14	799.7	R5	Microgabbro	51.79	16.14	8.16	0.15	8.04	11.41	3.54	0.06	0.57	0.06	0.0037	0.0064	0	99.94
131R-1, 11–16	803.6	11	Ferrogabbro	43.1	13.11	21.36	0.24	5.75	7.86	3.75	0.13	5.34	0.02	0.0079	0.0064	–0.48	100.2
137R-6, 112–119	859.4	R6	Microgabbro	48.88	16.01	12.24	0.20	8.75	9.49	3.43	0.07	1.07	0.17	0.0512	0.0245	–0.26	100.13
139R-1, 65–74	871.8	65	Olivine gabbro	50.5	20.95	5.62	0.09	8.35	11.19	3.42	0.04	0.23	0.01	0.0112	0.0143	–0.12	100.31
140R-1, 1–8	880.3	1	Olivine gabbro	51.01	13.61	8.53	0.16	10.27	13.45	2.56	0.04	0.6	0.01	0.0158	0.0133	–0.07	100.2
149R-2, 61–65	962.4	61	Microgabbro	51.92	18.28	4.61	0.09	7.93	13.85	3.11	0.03	0.32	0.01	0.0229	0.0102	–0.15	100.03
165R-3, 96–102	96.0	96	Olivine gabbro	51.68	17.44	6.37	0.11	8.84	12.57	3.2	0.04	0.36	0.01	0.008	0.0097	0.12	100.76
165R-3, 96–102	96.0	R3a	Olivine gabbro	51.23	16.94	5.64	0.11	9.28	13.51	2.82	0.02	0.28	0	0.0316	0.011	0.1	99.96
165R-4, 71–75	1109.3	71	Olivine gabbro	51.35	15.47	6.08	0.12	9.74	13.89	2.65	0.02	0.34	0	0.0194	0.0107	0.33	100.01
165R-4, 71–75	1109.3	71	Olivine gabbro	51.41	15.12	6.68	0.13	10.03	13.61	2.67	0.03	0.38	0.01	0.0155	0.0106	0.2	100.29
166R-2, 61–71	1112.7	61a	Olivine gabbro	52.58	22.76	3.46	0.06	4.82	11.94	4.17	0.04	0.2	0.01	0.0101	0.0056	0.03	100.08
169R-3, 108–118	1143.4	108	Olivine gabbro	52.04	16.68	6.62	0.12	8.93	12.36	3.26	0.04	0.42	0.01	0.006	0.0086	0.09	100.6
170R-7, 50–55	1158.0	R7	Microgabbro	49.96	17.55	7.01	0.12	10.06	11.52	3.05	0.04	0.3	0.03	0.0422	0.0142	0.9	100.59
178R-6, 132–138	1219.4	R6a	Microgabbro	49.67	15.09	10.5	0.18	7.83	11	2.98	0.07	1.63	0.17	0.0342	0.0129	0.05	99.23
183R-4, 13–17	1264.0	R4	Microgabbro	51.69	17.34	7.08	0.09	8.9	10.45	3.76	0.11	0.24	0	0.0056	0.0127	0.32	100.02
185R-1, 26–36	1279.1	26a	Olivine gabbro	49.26	15.06	8.17	0.14	12.86	11.71	2.38	0.02	0.26	0.01	0.0198	0.0207	0.21	100.11
188R-1, 31–35	1307.2	31	Olivine gabbro	51.79	16.1	7.37	0.14	9.03	12.14	3.33	0.04	0.35	0.01	0.0031	0.0076	0.23	100.52
191R-3, 61–67	1339.2	R3	Microgabbro	49.6	16.68	10	0.15	9.51	10.23	3.13	0.06	0.46	0.01	0.0589	0.0262	0.7	100.61
192R-1, 49–57	1345.8	49a	Olivine gabbro	48.58	17.63	9.48	0.15	10	10.85	2.92	0.05	0.41	0.01	0.0562	0.0277	0.12	100.27
198R-1, 25–30	1386.7	R1	Microgabbro	50.86	16.99	5.97	0.11	9.87	13.07	2.78	0.03	0.28	0.01	0.0385	0.0151	0.32	100.33
197R-3, 42–47	1386.7	R3b	Microgabbro	51.02	16.22	5.97	0.11	9.55	13.5	2.67	0.02	0.32	0	0.0212	0.0134	0.43	99.85
199R-6, 49–55	1400.1	49	Troctolitic gabbro	48.99	16.97	7.78	0.12	12.66	10.44	2.78	0.03	0.24	0.01	0.0126	0.0219	0.34	100.4
200R-1, 16–21	1402.2	16	Troctolitic gabbro	47	11.97	11.68	0.18	17.64	9.39	1.95	0.02	0.29	0.01	0.0159	0.0308	–0.2	99.98
202R-8, 7–16	1430.6	R8	Microgabbro	51.81	14.77	6.46	0.13	9.46	14.17	2.68	0.05	0.61	0.02	0.0272	0.0129	0	100.19

Table T1 (continued).

Core, section, interval (cm)	Depth (mbsf)	Thin section number	Rock type	Trace elements (ppm)															
				Mg#	Ca#	Sc	V	Cr	Co	Ni	Cu	Zn	Ga	Rb	Sr	Y	Zr	Nb	Ba
176-735B-																			
1R-1, 35–37	0.4	227	Olivine basalt	0.662	0.663	35	234	332	48	119	57	68	18	6	171	31	112	3	ND
16R-2, 5–10	63.1	219	Olivine gabbro	0.787	0.710	29	118	45	50	94	4	25	17	1	178	8	13	2	9
16R-5, 38–40	66.8	220	Olivine microgabbro	0.819	0.739	32	115	1354	35	249	5	48	11	1	149	9	16	1	10
23R-5, 3–5	104.9	232	Diabase	0.769	0.671	35	263	246	45	100	50	83	19	2	152	36	131	4	ND
25R-2, 104–107	113.3	234	Olivine gabbro	0.809	0.730	37	136	414	34	159	40	29	13	1	143	10	17	2	10
38R-2, 24–26	182.5	257	Troctolitic micrograbbro	0.683	0.670	29	160	356	48	173	31	63	16	1	182	18	44	2	7
41R-4, 22–27	199.7	260	Olivine gabbro	0.692	0.620	42	195	9	37	39	30	41	16	2	163	14	20	2	6
50R-1, 82–90	238.8	272	Oxide gabbro	0.392	0.625	56	896	ND	77	34	82	109	18	2	123	21	83	5	ND
51R-2, 16–25	244.5	274	Oxide gabbro	0.320	0.558	44	1383	ND	75	29	84	145	25	3	148	17	58	4	ND
74R-6, 115–119	382.9	200	Olivine microgabbro	0.548	0.591	37	302	181	41	58	41	87	21	2	161	35	90	2	ND
83R-7, 115–120	461.1	213	Troctolite	0.860	0.762	10	44	621	118	938	69	62	7	2	73	3	7	1	5
90R-1, 126–137	509.1	126	Troctolitic gabbro	0.832	0.728	13	42	211	45	271	65	34	13	1	165	4	11	2	1
90R-6, 28–38	514.8	28	Troctolitic gabbro	0.853	0.749	19	68	667	58	393	84	41	10	1	133	7	16	2	11
90R-8, 47–52	517.3	47	Olivine gabbro	0.845	0.706	9	34	69	68	409	37	42	12	1	148	4	11	2	10
91R-1, 43–53	517.8	43	Troctolitic gabbro	0.846	0.785	22	90	1012	54	393	47	35	11	1	145	8	23	2	8
91R-2, 26–32	519.0	26	Troctolitic gabbro	0.711	0.635	71	243	610	46	170	93	85	14	2	70	92	210	3	5
91R-2, 101–110	519.8	101	Troctolitic gabbro	0.797	0.688	8	37	43	58	313	47	53	13	2	150	6	16	1	10
95R-2, 93–97	546.9	R2	Troctolitic gabbro	0.683	0.615	37	182	14	38	33	21	47	19	1	175	13	16	2	10
96R-1, 25–33	548.9	R1a	Microgabbro	0.705	0.626	42	177	12	39	32	21	48	15	2	168	13	26	2	14
96R-1, 82–84	549.1	R1b	Microgabbro	0.718	0.827	40	167	14	42	36	25	42	17	2	170	13	16	1	11
121R-1, 14–19	719.8	R1c	Olivine gabbro	0.813	0.742	43	161	223	34	102	95	36	14	0	154	11	17	1	6
121R-3, 65–75	723.3	65a	Microgabbro	0.755	0.668	38	156	172	36	91	8	34	16	1	160	19	41	2	1
123R-4, 83–89	744.0	R4a	Troctolitic gabbro	0.779	0.687	28	94	251	46	130	70	40	15	1	174	8	23	1	11
128R-3, 6–12	777.5	6	Microgabbro	0.78	0.733	38	148	322	39	104	95	38	14	1	148	10	12	2	8
130R-5, 10–14	799.7	R5	Microgabbro	0.697	0.640	38	171	15	41	40	21	48	17	0	172	19	45	2	10
131R-1, 11–16	803.6	11	Ferrogabbro	0.386	0.537	32	844	10	54	52	60	156	26	2	160	24	76	3	ND
137R-6, 112–119	859.4	R6	Microgabbro	0.625	0.605	28	148	367	48	173	37	85	18	1	154	36	147	2	0
139R-1, 65–74	871.8	65	Olivine gabbro	0.776	0.644	29	103	70	49	87	73	44	15	1	165	9	16	2	12
140R-1, 1–8	880.3	1	Olivine gabbro	0.737	0.744	50	221	101	41	86	70	50	14	2	134	16	26	2	11
149R-2, 61–65	962.4	61	Microgabbro	0.800	0.711	41	165	19	39	56	72	40	15	1	167	11	14	1	11
165R-3, 96–102	96.0	96	Olivine gabbro	0.764	0.685	17	59	65	18	36	36	21	18	1	215	5	10	1	9
165R-3, 96–102	96.0	R3a	Olivine gabbro	0.793	0.726	40	145	209	35	78	98	30	13	1	155	9	13	2	9
165R-4, 71–75	1109.3	71	Olivine gabbro	0.789	0.743	38	146	106	34	68	58	32	14	2	143	11	13	1	7
165R-4, 71–75	1109.3	71	Olivine gabbro	0.778	0.738														
166R-2, 61–71	1112.7	61a	Olivine gabbro	0.765	0.613	35	128	51	35	63	62	35	17	1	168	10	16	1	4
169R-3, 108–118	1143.4	108	Olivine gabbro	0.759	0.677	31	140	34	31	61	58	37	15	1	181	12	18	1	13
170R-7, 50–55	1158.0	R7	Microgabbro	0.770	0.676														
178R-6, 132–138	1219.4	R6a	Microgabbro	0.635	0.671	28	124	375	46	147	91	40	16	1	171	9	13	2	8
183R-4, 13–17	1264.0	R4	Microgabbro	0.746	0.606	34	124	216	39	103	49	34	13	1	163	8	15	1	4
185R-1, 26–36	1279.1	26a	Olivine gabbro	0.786	0.731	34	114	130	54	143	72	43	13	1	146	7	12	2	11
188R-1, 31–35	1307.2	31	Olivine gabbro	0.741	0.668	38	135	168	28	75	56	27	15	1	174	9	13	2	8
191R-3, 61–67	1339.2	R3	Microgabbro	0.689	0.644	25	151	383	56	181	60	60	18	1	181	15	27	2	9
192R-1, 49–57	1345.8	49a	Olivine gabbro	0.711	0.672	50	203	182	36	90	92	38	15	1	145	20	45	2	7
198R-1, 25–30	1386.7	R1	Microgabbro	0.794	0.722	37	137	274	41	104	79	31	14	1	169	9	12	1	10
197R-3, 42–47	1386.7	R3b	Microgabbro	0.789	0.736	39	159	148	37	92	77	33	14	1	164	10	12	2	8
199R-6, 49–55	1400.1	49	Troctolitic gabbro	0.791	0.675	22	88	94	58	158	101	46	13	1	161	6	13	2	3
200R-1, 16–21	1402.2	16	Troctolitic gabbro	0.779	0.727	30	111	114	82	230	116	71	11	1	116	8	14	1	16
202R-8, 7–16	1430.6	R8	Microgabbro	0.774	0.745	31	124	356	50	181	12	53	18	1	162	15	23	2	6

Table T1 (continued).

Core, section, interval (cm)	Depth (mbsf)	Thin section number	Rock type	Major element oxides (wt%)													
				SiO_2	Al_2O_3	Fe_2O_3	MnO	MgO	CaO	Na_2O	K_2O	TiO_2	P_2O_5	Cr_2O_3	NiO	LOI	Total
203R-1, 5–17	1430.9	5	Melanogabbro	46.34	19.63	7.84	0.11	12.93	9.71	2.29	0.1	0.22	0.01	0.0062	0.0472	1.01	100.26
203R-3, 17–26	1433.3	17	Olivine gabbro	48.66	16.04	8.15	0.13	12.98	10.92	2.42	0.02	0.25	0.01	0.0185	0.0217	0.44	100.06
203R-5, 22–31	1436.1	22	Olivine gabbro	51.29	17.06	5.2	0.1	9.65	13.6	2.66	0.02	0.27	0.01	0.0267	0.0126	0.7	100.6
204R-1, 55–64	1441.1	55	Troctolitic gabbro	50.3	16.87	7.69	0.13	10.33	11.5	3.11	0.04	0.31	0.01	0.0104	0.0128	0.32	100.64
205R-1, 38–46	1450.6	38	Troctolitic gabbro	50.76	19.15	5.69	0.09	9.15	11.89	3.15	0.03	0.25	0.01	0.0117	0.0139	0.48	100.68
206R-2, 46–52	1461.4	46	Olivine gabbro	50.78	17.86	5.63	0.1	9.01	12.96	2.8	0.03	0.34	0.01	0.0242	0.0125	0.11	99.66
206R-6, 142–146	1467.8	142	Olivine gabbro	48.95	17	7.7	0.12	12.27	10.86	2.55	0.03	0.2	0.01	0.0186	0.025	0.23	99.95
207R-3, 32–41	1472.0	32	Olivine gabbro	51.03	16.78	5.63	0.1	9.67	13.53	2.64	0.03	0.34	0.01	0.0214	0.0126	1.2	101.01
207R-3, 88–98	1472.8	88	Melanogabbro	49.3	14.57	8.08	0.13	12.85	11.99	2.35	0.03	0.36	0.01	0.0163	0.0228	0.21	99.92
207R-4, 20–29	1473.3	20	Olivine gabbro	50.05	18.8	6.33	0.1	9.82	11.51	3.05	0.04	0.25	0.01	0.0157	0.0159	0.35	100.34
207R-4, 64–70	1473.7	R4b	Olivine gabbro	50.94	17.21	5.59	0.1	9.74	13.39	2.81	0.03	0.32	0.01	0.0282	0.0132	0.39	100.56
209R-2, 66–71	1490.4	R2A	Olivine gabbro	51.11	16.05	6.35	0.12	9.72	13.33	2.74	0.03	0.35	0.01	0.0314	0.0149	0.2	100.06
209R-3, 24–32	1491.4	24	Troctolitic gabbro	46.82	13.88	10.42	0.15	16.78	8.82	2.22	0.02	0.18	0.01	0.0092	0.027	0.72	100.05
Muds:																	
2, 9–140				50.26	16.35	8	0.13	8.4	11.73	3.32	0.09	0.65	0.09	0.02	0.0195	1.23	100.31
3, 4–170				51.06	15.8	7.79	0.14	9.48	12.28	3.05	0.05	0.56	0.03	0.0123	0.0136	0.15	100.41
4, 0–208				50.6	16.75	6.33	0.11	9.45	12.86	2.92	0.05	0.39	0.03	0.0224	0.0192	0.72	100.26
BCR-1:																	
Point samples:																	
Average				49.51	16.29	8.18	0.13	10.4	11.56	2.87	0.05	0.81	0.02	0.03	0.02	0.38	100.25
Standard deviation				2.92	2.52	3.81	0.04	3.61	1.81	0.59	0.04	1.84	0.04	0.03	0.02	0.48	0.53
Maximum				52.83	22.76	24.08	0.28	29.08	15.16	4.17	0.22	11.39	0.17	0.1732	0.1245	1.79	102.6
Minimum				38.87	7.69	3.46	0.06	4.82	5.84	1.01	0.02	0.1	0	0.0026	0.0039	–0.51	99.19

Notes: LOI = loss on ignition. ND = not detected. Mg# = $Mg^{2+}/(Mg^{2+} + Fe^{2+})$.

Table T1 (continued).

Core, section, interval (cm)	Depth (mbsf)	Thin section number	Rock type	Trace elements (ppm)														
				Mg#	Ca#	Sc	V	Cr	Co	Ni	Cu	Zn	Ga	Rb	Sr	Y	Zr	Nb	Ba
203R-1, 5–17	1430.9	5	Melanogabbro	0.794	0.701	11	52	46	53	336	53	55	14	1	153	6	15	2	9
203R-3, 17–26	1433.3	17	Olivine gabbro	0.788	0.714	28	98	129	59	149	56	47	13	2	147	7	14	2	9
203R-5, 22–31	1436.1	22	Olivine gabbro	0.812	0.739	35	127	186	34	90	50	32	14	1	164	9	16	1	9
204R-1, 55–64	1441.1	55	Troctolitic gabbro	0.758	0.671	17	60	75	41	104	58	36	15	2	202	5	11	2	9
205R-1, 38–46	1450.6	38	Troctolitic gabbro	0.789	0.676	24	88	107	45	117	84	39	15	1	181	7	12	2	3
206R-2, 46–52	1461.4	46	Olivine gabbro	0.789	0.719	32	122	170	36	90	53	36	15	0	172	10	18	1	11
206R-6, 142–146	1467.8	142	Olivine gabbro	0.788	0.702	24	84	132	58	175	201	46	13	0	161	7	10	1	9
207R-3, 32–41	1472.0	32	Olivine gabbro	0.800	0.739	37	137	143	33	89	57	31	15	0	162	11	16	1	6
207R-3, 88–98	1472.8	88	Melanogabbro	0.788	0.738	34	126	102	48	147	97	45	13	2	138	10	18	2	6
207R-4, 20–29	1473.3	20	Olivine gabbro	0.783	0.676	25	81	74	36	96	63	33	15	1	185	7	12	2	8
207R-4, 64–70	1473.7	R4b	Olivine gabbro	0.803	0.725	39	141	191	34	97	99	26	13	1	157	9	12	2	9
209R-2, 66–71	1490.4	R2A	Olivine gabbro	0.781	0.729	40	144	200	32	91	88	29	13	2	155	9	13	2	6
209R-3, 24–32	1491.4	24	Troctolitic gabbro	0.790	0.687	19	70	65	75	196	37	59	12	1	137	6	9	1	12
Muds:																			
2, 9–140				0.710	0.661	40	169	144	79	144	89	135	16	1	171	23	85	2	488
3, 4–170				0.739	0.690	39	171	87	136	93	54	63	15	1	160	17	56	2	63
4, 0–208				0.777	0.709	39	152	160	161	144	87	79	14	1	165	13	31	2	159
BCR-1:						29	386	2	37	12	28	128	23	50	334	37	194	13	690
Point samples:																			
Average				0.744	0.690	32	178	216	47	145	62	49	15	1	157	13	30	2	8
Standard deviation				0.104	0.055	11	216	243	16	139	32	26	3	1	24	13	38	1	3
Maximum				0.860	0.827	71	1383	1354	118	938	201	156	26	6	215	92	210	5	16
Minimum						8	34	9	18	29	4	21	7	0	70	3	7	1	0